Biometals
DOI 10.1007/s10534-017-0039-5

Triphenylphosphonium-desferrioxamine as a candidate mitochondrial iron chelator

Roxana Y. P. Alta · Hector A. Vitorino · Dibakar Goswami · M. Terêsa Machini · Breno P. Espósito

Received: 5 July 2017 / Accepted: 28 July 2017

Abstract Cell-impermeant iron chelator desferrioxamine (DFO) can have access to organelles if appended to suitable vectors. Mitochondria are important targets for the treatment of iron overload-related neurodegenerative diseases. Triphenylphosphonium (TPP) is a delocalized lipophilic cation used to ferry molecules to mitochondria. Here we report the synthesis and characterization of the conjugate TPP–DFO as a mitochondrial iron chelator. TPP–DFO maintained both a high affinity for iron and the antioxidant activity when compared to parent DFO. TPP–DFO was less toxic than TPP alone to A2780 cells ($IC_{50} = 135.60 \pm 1.08$ and $4.34 \pm 1.06\ \mu mol\ L^{-1}$, respectively) and its native fluorescence was used to assess its mitochondrial localization ($Rr = +0.56$). These results suggest that TPP–DFO could be an interesting alternative for the treatment of mitochondrial iron overload e.g. in Friedreich's ataxia.

Keywords Iron overload · Antioxidant · Mitochondria · Triphenylphosphonium

Introduction

Mitochondria are major sites for heme and iron–sulfur cluster synthesis and consequently there is a constant iron influx into these organelles. Also, they are a major source of the superoxide anion, O_2^- (Ma et al. 2014). Mitochondria have many essential roles for cell survival and their dysfunction contributes to a wide range of diseases (Murphy and Smith 2000), including Friedreich's ataxia (Puccio et al. 2001), Parkinson's disease, diabetes, Huntington's disease (Nishikawa et al. 2000), disorders associated with mitochondrial DNA mutations (Pitkanen and Robinson 1996), and degenerative diseases associated with aging (Smith et al. 2003a, b).

The design of a cell-permeable vector efficiently targeted to mitochondria is a challenge due to the their imperviousness to a wide range of molecules (Rin Jean et al. 2014). One of the strategies for the transport of bioactive molecules to mitochondria

Electronic supplementary material The online version of this article (doi:10.1007/s10534-017-0039-5) contains supplementary material, which is available to authorized users.

R. Y. P. Alta (✉) · H. A. Vitorino · B. P. Espósito
Laboratory of Bioinorganic Chemistry and Metallodrugs, Department of Fundamental Chemistry, University of São Paulo, Av. Lineu Prestes 748, São Paulo 05508-000, São Paulo, Brazil
e-mail: rpastranaa@uni.pe

R. Y. P. Alta · M. Terêsa Machini
Laboratory of Peptide Chemistry, Department of Biochemistry, Institute of Chemistry, University of São Paulo, Av. Professor Lineu Prestes 748, São Paulo 05508-000, São Paulo, Brazil

D. Goswami
Bhabha Atomic Research Centre, Mumbai, India

Published online: 02 August 2017

involve the use of delocalized lipophilic cations (DLC), including the triphenylphosphonium cation (TPP), which has been widely used for the delivery of therapeutic cargoes to this organelle (Smith et al. 2011; Mourtada et al. 2013) such as antioxidant agents (Smith et al. 2003a; Filipovska et al. 2005; Ross et al. 2005), peptide and peptide nucleic acids (PNAs) (Ross et al. 2004; Kolevzon et al. 2011). Selected therapies that benefit from TPP-delivered molecules include photodynamic therapy (Lei et al. 2010), modulation of the mechanism of cell death (Malouitre et al. 2010; Mourtada et al. 2013) and increasing energy expenditure for obesity treatments (Lou et al. 2007).

The lipophilic cation TPP binds covalently to biologically active molecules (Supplementary Information, Figure S1), accumulating ca. 5–10 times within the cytoplasm through the plasma membrane potential ($\Delta\psi p$), and continuing to accumulate within the mitochondrial matrix by a factor of 100–500 through the mitochondrial membrane potential ($\Delta\psi m$). TPP-cargo conjugates can cross directly lipid bilayers from all types of mitochondria including in the brain (Murphy and Smith 2000).

Desferrioxamine (DFO) is a bacterial siderophore with high selectivity for iron. It is a hexadentate chelator with antioxidant, anti-proliferative and anti-tumor (Kalinowski and Richardson 2005) activities. It was the first clinically used drug for the treatment of iron overload disorders, but its low cell penetration and bioavailability (high hydrophilicity and molecular weight) make the drug unavailable orally, being administered as long, uncomfortable intravenous or subcutaneous infusions. Other chelators that act at the cellular level (Goswami et al. 2014, 2015) such as deferiprone or deferasirox are still being pursued.

In our previous works, DFO has been directed to cells through antioxidant molecules (caffeine) (Alta et al. 2014), cell penetrating peptides (CPP) (Goswami et al. 2015) and mitochondria penetrating peptide (MPP) (Horton et al. 2008; Alta et al. 2017). Here, our aim was to link a DLC vector that does not interfere with the iron chelation moiety of DFO in order to create a conjugate (TPP–DFO) with cellular and mitochondrial penetration for the treatment of mitochondrial iron overload. Conjugation was achieved by Schiff reaction between the amine (DFO) and an aldehyde ((formylmethyl) triphenylphosphonium, FTP).

Materials and methods

Materials

FTP, trifluoroacetic acid (TFA), HEPES, NTA, FAS (ferrous ammonium sulfate hexahydrate), ascorbic acid, calcein were purchased from Sigma-Aldrich (USA). Dihydrorhodamine (DHR) was obtained from Biotium (USA) and DFO mesylate (Desferal) was donated by Cristália (Brazil). The solvents dimethylformamide (DMF), chloroform, benzene (analytical grade) and acetonitrile (ACN) (chromatographic grade) were purchased from Vetec Fine Chemicals Ltd. (Brazil). HBS (Hepes Buffered Saline; NaCl 150 mmol L^{-1}, HEPES 20 mmol L^{-1}; pH 7.4; treated with Chelex-100 purchased from Sigma, 1 g/100 mL) was used throughout the experiments.

Synthesis, purification and characterization of TPP–DFO

Synthesis, purification and chemical characterization: The method used was modified from previous reports (Wittig and Schoch-Grübler 1978). In a round bottom flask, a solution of FTP (0.65 mmol) dissolved in 20 mL of chloroform was treated dropwise with a solution DFO (0.185 mmol) in 5 mL DMF. The mixture was refluxed at 140 °C under stirring for 20 h. The water formed as byproduct was removed with a Soxhlet extractor. The solvents were removed in a rotary evaporator. The brown product was washed several times with benzene and water and was recrystallized from chloroform/ethyl acetate (3:1).

The reaction product was analyzed by reverse-phase high performance liquid chromatography (RP-HPLC) coupled to liquid chromatography electrospray ionization mass spectrometry (LC/ESI–MS) and purified by semi-preparative RP-HPLC. Eluents in both cases were: solvent A: 0.1% TFA/H_2O, solvent B: 60% ACN/0.09% TFA in H_2O and solvent B^C: 80% ACN/0.09% TFA in H_2O. (Supplementary Information, Figure S2).

Analytical RP-HPLC was performed in an LDC system composed of an automatic gradient controller, two pumps (LDC Analytical, a ConstaMetric 3500 and a ConstaMetric 3200 pump), a UV detector (Milton Roy SpectroMonitor 3100), a manual sample injector (Rhysodine 7125), an integrator (TermoSeparation

Products, Data Jet integrator) and a Grace C18 column, 5 μm, 300 Å, 0.46 × 25 cm). A volume of 10 μL of a 1 g L^{-1} of the reaction product dissolved in solvent B^C was injected. Elution occurred under the following conditions: linear gradient 5–95% of solvent B for 60 min, wavelength of 210 nm, flow rate of 1 mL/min.

LC/ESI–MS using the conditions described above was performed on a Shimadzu liquid chromatographer (Kyoto, Japan) composed of two LC-20AD pumps, a DGU-20A3 degasser, a CTO-20A column oven, a C18 Shim-pack GVP-ODS precolumn, a C18 Shim-pack VP-ODS column, and SDP-20AV detector coupled to AmaZon X electrospray mass spectrometer (Bruker Daltonics, Fahrenheitstrasse, Germany). The software HyStar 3.2 was used to analyze the mass spectra obtained.

Semi-preparative RP-HPLC employed a Grace C18 column 5 μm, 300 Å, 1 × 25 cm). The following linear gradient was applied: 30% B for 10 min, 30 to 90% in 70 min and 90 to 95% B. The flow rate was at 3.0 mL min^{-1} and detection was at 210 nm; The fractions were collected, analyzed, those containing the product with high purity degree were pooled and lyophilized. The solid purified product was dissolved in water for further analysis by LC/ESI–MS using the equipment and analytical conditions cited above. The results were in agreement with the calculated molar mass.

Identity of purified TPP–DFO was also confirmed by ^{1}H nuclear magnetic resonance spectroscopy in d_6-DMSO at 298 K, acquired using a Bruker model A3, 500 MHz spectrometer. δ 1.0–1.6 ppm (18H, m, $–CH_2–$), δ 1.97 ppm (3H, s, $–CH_3$), δ 2.29–3.01 ppm (12H, m, $–CO–CH_2–$), δ 7.85 ppm (3H, m, –NH–CO–), δ 7.68–7.98 ppm (15H, m, –CH–), δ 8.33 ppm (H, m, –CH=N–), δ 9.67 ppm (3H, m, –N–OH) (Supplementary Information, Figure S3). Finally, the resulting fluorescent probe TPP–DFO was characterized by UV absorption and fluorescence spectroscopy in aqueous medium (50 μmol L^{-1}).

Antioxidant activity

The pro-oxidant standard Fe(NTA) (1:3 Fe:NTA molar ratio) was prepared by adding FAS to a stock solution of aqueous NTA (dissolved in HBS buffer), and allowed to react for 1 h at 37 °C. In a flat, transparent 96-well microplate, it was placed 10 μL of 20 μmol L^{-1} chelators (DFO, TPP–DFO) and 10 μL of Fe(NTA) at 0–10 μmol L^{-1}. Then, the samples received 180 μL of a mixture of 40 μmol L^{-1} ascorbic acid, 50 μmol L^{-1}DHR in HBS at 37 °C. Assays were performed in triplicate. Fluorescence was registered in a BMG FluoStar Optima instrument for 60 min at 37 °C ($\lambda_{exc}/\lambda_{em}$ = 485/520 nm). The slopes of the curves (indicating the rate of DHR oxidation, presented in fluorescence units per minute) were calculated from 15 to 40 min and were plotted against iron concentration (Esposito et al. 2003; Alta et al. 2014).

Competition studies with calcein

Aliquots of 180 μL of calcein (2 μmol L^{-1} in HBS Buffer) were placed in flat, transparent 96-well microplates and the fluorescence was recorded at 37 °C on a BMG FluoStar Optima instrument ($\lambda_{exc}/\lambda_{em}$ = 485/520 nm) for 10 min. After that, 10 μL FAS (ferrous ammonium sulfate, 2 μmol L^{-1} in water, final concentration) was added to the wells, and the reaction was allowed to proceed at 37 °C until the fluorescence quenching was stabilized (10 min). The calcein-iron (CAFe) species thus formed in solution was treated with 10 μL aliquots of test compounds (TPP–DFO and DFO) at increasing concentrations, and fluorescence was further recorded until stabilization (60 min) (Espósito et al. 2002).

In vitro studies

Cell culture

A2780 (ovarian cancer) cell line was obtained from Fox Chase Cancer Center and cultured in RPMI-1640 medium supplemented with 10% FBS (Fetal Bovine Serum) and 1% penicillin/streptomycin. Cells were incubated at 37 °C in a humidified incubator with 5% CO_2.

Cytotoxicity assays

A2780 cells were plated in 96-well flat-bottom tissue culture plates (Starstedt) at 25,000 cells per well, with DFO, FTP and TP-DFO using a previously described protocol (Wilson and Lippard 2012). The culture media was removed, and cells were washed (Alta et al. 2017). Incubations were conducted in cell-appropriate medium. Cellular viability was analyzed

after an overnight incubation at 37 °C with 5% CO_2 using the CCK-8 viability dye (Dojindo, Rockville, Maryland) at an absorbance of 450 nm. From the resulting dose–response curves, 50% growth inhibitory concentration (IC_{50}) values were determined by interpolation.

Cell imaging studies

A2780 cells were seeded in an imaging dish in 2 mL of growth medium at 60% confluence. The growth medium was substituted by medium containing 2–8 μmol L^{-1} of TPP–DFO or 2 μmol L^{-1} of FTP, and the cells were incubated for 1 h. MitoTracker Green was added to cells at 1 μmol L^{-1} and allowed to incubate for 30 min. At the end of the incubation period, the medium was aspirated, and the cells were washed three times with 1 mL PBS and then treated with 2 mL of dye-free DMEM. The imaging experiments were performed using a Zeiss Axiovert 200 M inverted epifluorescence microscope equipped with an EM-CCD digital camera (Hamamatsu) and a MS200 XY Piezo Z stage (Applied Scientific Instruments). The light source was an X-Cite 120 metal-halide lamp (EXFO), and the fluorescence images were obtained with an oil-immersion objective at ×63 magnification. The microscope was operated by the Volocity software program of Perkin-Elmer. Colocalization of the dyes was quantitated with the software ImageJ (Horton et al. 2008) using a previously described protocol (Fonseca et al. 2011; Wisnovsky et al. 2013).

Results and discussion

Synthesis, purification and characterization of TPP–DFO

The conjugation of active biomolecules to TPP usually occur through a simple S_N2 reaction (Rin Jean et al. 2014) forming a covalent bond between TPP and an alkyl chain (Murphy and Smith 2000). The aldehyde derivative FTP can also react specifically with primary amines for the formation of imines or enamines (Wittig and Schoch-Grübler 1978).

TPP has a single positive charge that is stabilized through resonance by the three phenyl groups. In addition, the large hydrophobic surface of TPP allows favorable interaction with the inner mitochondrial membranes (IMM), whose negative membrane potential (−150 to −180 mV) is lower than the plasma membrane potential (−30 to −60 mV) (Liberman et al. 1969). This property certainly allows the absorption of TPP in the mitochondrial matrix, where it is freely soluble or adsorbed in the inner fold depending upon the total hydrophobicity (Murphy and Smith 2007; Smith et al. 2012), leading to accumulation within mitochondria in rates higher than 90% (Smith et al. 2003b).

Many of the reactions between FTP and primary amines can produce condensation products, enamines, decreasing the possibility of obtaining Schiff bases (Wittig and Schoch-Grübler 1978) (Fig. 1a). Aldehydes in general present keto-enol tautomerism, which is an easily reversible process. By capturing one hydrogen atom from the adjacent carbon FTP gives rise to an intramolecular reaction for double bond formation and insertion of a hydroxyl function, or an enol(Wade 2003). The carbonyl group (C=O) of FTP provides polarity to the molecule. Figure 1b shows the structures of the precursor FTP and the product formed TPP–DFO.

TPP–DFO was purified in a semi-preparative scale by RP–HPLC with a yield of 38.3%, which is in the range of the expected yields for RP-HPLC for this type large and relatively amphipathic compound. In fact, it has a higher retention time than DFO but similar to the retention times of other DFO conjugates with lipophilicity similar to TPP (Wade 2003; Smith et al. 2011). Its purity percentage was higher than 95%.

Electrospray ionization (ESI) of TPP-DFO resulted in three major ions (Table 1 and Figure S2). The species $[2M + 2H]^+$ and $[2M + H_2O]^+$ is consistent with other DFO conjugates (DFOB-MPOAc) (Liu et al. 2010) having predominant species such as $[2M + H_2O]^+$ and $[2M + Na^+]$ (Waters 1999; Abián et al. 2008).

The ^1H NMR spectrum of TPP–DFO reaffirmed that formed structure is an imine (Figure S3A) with a major peak at δ 8.33 ppm characteristic of a Schiff base hydrogen, in good agreement with previous

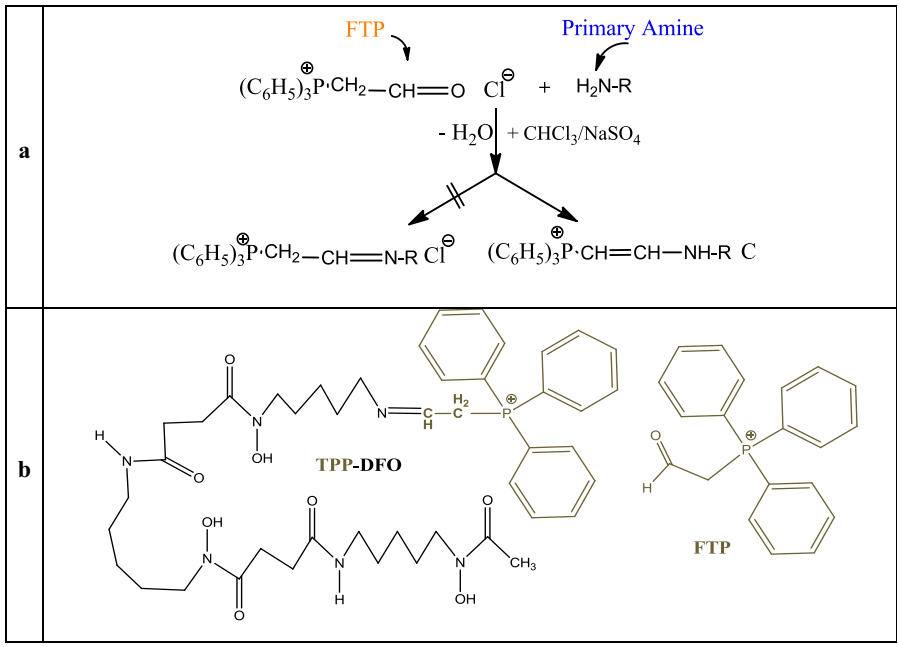

Fig. 1 **a** Reaction of the triphenylphosphonium aldehyde (FTP) with a primary amine (e.g., DFO) and **b** structure of the compounds: TPP-DFO and FTP precursor

Table 1 ESI/MS data for TPP-DFO, molar masses (Mw; g mol^{-1}) and charges of the detected ions

MOLECULE	Ion [M]	Species	Mw (g mol^{-1}) Calculated	Mw (g mol^{-1}) Experimental
TPP-DFO	$[C_{19}H_{18}P]^{+}$	$[M]^{+}$	278.8	279.2
	$[C_{28}H_{53}N_5O_6]^{2+}$	$[2M + 2H]^{2+}$	554.7	557.2
	$[C_{44}H_{68}N_6O_9P]^{2+}$	$[2M + H_2O]^{2+}$	856.0	856.9

results (Gottlieb et al. 1997; Suresh et al. 2013) and software simulations (Figure S3B).

Antioxidant activity

Under physiological conditions, ascorbate and labile iron may generate ROS in plasma (Esposito et al. 2003), cytosol (Goswami et al. 2014) and mitochondria (Cabantchik 2014). Therefore, clinical chelators for the treatment of iron overload have to suppress any iron-catalyzed oxidation. Assessing the suppressing effect of a chelator on the oxidation rate of DHR induced by iron/ascorbate is a convenient method to verify its antioxidant activity[35]. The rate decrease caused by TPP–DFO and DFO (positive control) displayed in Fig. 2 indicates that both were effective antioxidants. There is a positive correlation between the number of hydroxamate moieties in the DFO structure and antioxidant activity, indicating that strong iron chelation is directly associated with this property (Baccan et al. 2012). DFO contains three hydroxamate groups that coordinate iron in a hexadentate complex. The antioxidant activity of TPP–DFO indicates that both strong iron affinity and binding stoichiometry were preserved.

Competition studies with calcein

The fluorophore calcein (CA) is extensively used as an iron probe for the quantification of non-transferrin-bound iron (NTBI) (Espósito et al. 2002). Initially, iron complexing with calcein causes stoichiometric fluorescence quenching of this molecule (Goswami et al. 2014, 2015). When iron is added in ferrous form, it quickly oxidizes to Fe(III) because the stability constant CAFe is higher (log $K_{CAFe} = 33.9$) (Vitorino et al. 2015) due to the fact that hard donors (O) interact better with the hard acid Fe(III). This ion has a greater affinity to DFO (log $K_{DFO\text{-}Fe} = 42.33$) (Domagal-Goldaman et al. 2009) than to calcein.

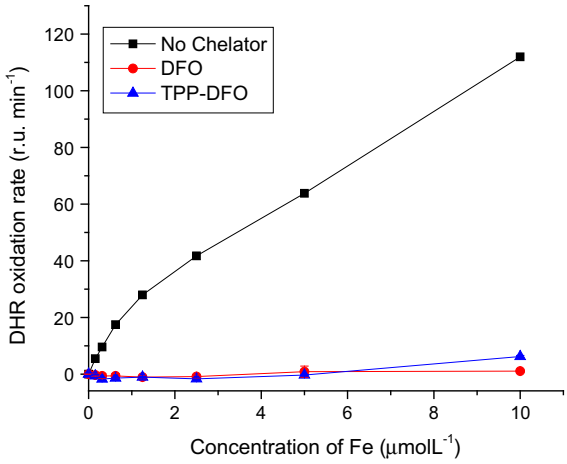

Fig. 2 Effect of the chelators (20 μmol L^{-1}) on the rate of DHR oxidation catalyzed by iron/ascorbate in HBS for 1 h at 37 °C. Results are the average of triplicates and representative of at least two independent experiments. *r.u.* relative fluorescence units

Therefore, DFO is able to regenerate the fluorescence of CA through a competitive equilibrium with CAFe (Espósito et al. 2002). Thus, it is a form to check whether the conjugation of TPP preserves the chelating ability of DFO.

Competition studies with calcein and TPP–DFO were conducted in order to determine the apparent stability constant (K_{app}) of the respective iron complexes in a physiologically relevant medium (Fig. 3).

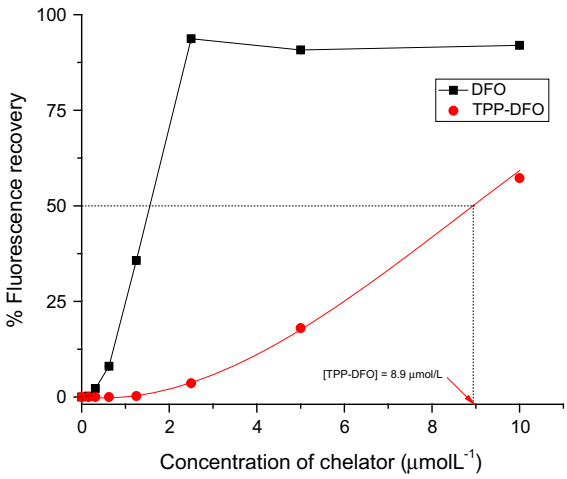

Fig. 3 Fluorescence recovery (%) as a function of chelator concentration in HBS/Chelex buffer (pH 7.4) for 1 h and 37 °C. Results are the average of triplicate experiments of at least two independent experiments (time 24 h)

Stoichiometric (1:1) quenching of calcein fluorescence by iron is fast. Treatment of the calcein-iron complex with increasing amounts of TPP–DFO leads to a steady recovery of the fluorescence. The equilibria involved are (Eqs. 1–3):

$$\mathrm{CAFe} \rightleftharpoons \mathrm{CA} + \mathrm{Fe} \qquad K_{diss} \tag{1}$$

$$\mathrm{Fe} + \mathrm{TPP{-}DFO} \rightleftharpoons \mathrm{Fe\,(TPP{-}DFO)} \qquad K_{app} \tag{2}$$

$$\mathrm{CAFe} + \mathrm{TPP{-}DFO} \rightleftharpoons \mathrm{Fe\ (TPP{-}DFO)} + \mathrm{CA}$$

$$K = K_{diss} \cdot K_{app} \tag{3}$$

The expression for K is given by Eq. (4):

$$K = \frac{[\mathrm{CA}][\mathrm{Fe(TPP{-}DFO)}]}{[\mathrm{CaFe}][\ \mathrm{TPP{-}DFO}]} \tag{4}$$

A plot of the fluorescence recovery by the end of the experiment as a function of TPP–DFO concentration (Fig. 3) indicates that for [TPP–DFO] = 8.9 μmol L^{-1} there is a 50% fluorescence recovery, indicating that half of the calcein is binding with iron and thus in this situation [CA] = [CAFe]. Notice for DFO the probe is saturated (Fig. 3 and S4B), because there is greater iron affinity for DFO (greater stability constant) than for calcein, for this reason, it is not feasible to calculate a K_{app} to Fe–DFO. Therefore, half (1 μmol L^{-1}) of the original iron is complexed by the TPP–DFO as Fe(TPP–DFO). Substitution of these figures in Eq. (4) for the chelator and assuming the effective K_{diss}(Vitorino et al. 2015) to be $1 \times 10^{-33.9}$, log K_{app} can thus be estimated as Fe(TPP–DFO) = 32.95. K_{app} indicates that TPP–DFO affinity for with iron is very high, only one order of magnitude lower than CAFe. Compared to the parent DFO, the decreased affinity may be related to disturbance in the coordination moiety caused by the bulky TPP substituent. Nevertheless, TPP–DFO is still a very good iron scavenger under these conditions, which explains its observed role as an antioxidant due to the immobilization of iron in stable, redox-inactive forms that are of great interest for chelation therapy.

Cytotoxicity studies

The toxicity of TPP–DFO was along with that of its building parts (FTP and DFO) in A2780 cells (Table 2 and Figure S5). TPP–DFO was ten times more toxic than DFO and 30 times less toxic than FTP. DFO is poorly cell permeable, therefore any strategy that

Table 2 Cell viability of TPP-DFO and its precursors against A2780 cells after 24 h

COMPOUNDS	IC_{50} (μmol L^{-1})
FTP	4.34 ± 1.06
DFO	1452.00 ± 1.13
TPP–DFO	135.60 ± 1.08

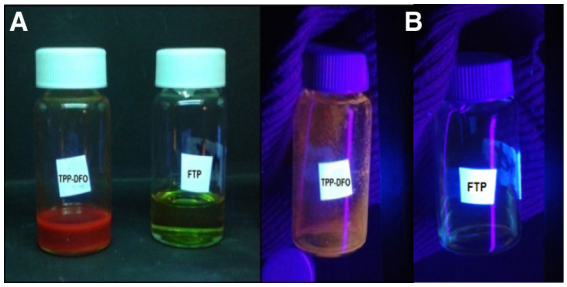

Fig. 4 **a** TPP-DFO and FTP compound, **b** fluorescence under UV light (UV, $\lambda_{Ex} = 365$ nm)

delivers this strong metal chelator within a cell is expected to raise its toxicity by the disruption of the homeostasis of other ions [e.g. Zn(II)]. However, TPP–DFO is not as toxic as FTP alone. Also, TPP–DFO has a very high IC_{50}, on the range of 10^2 μmol L^{-1}, well above typical therapeutic concentrations. These facts point to a well-tolerated chelator.

DFO bound to TPP leads to a conjugate less toxic to A2780 cells than when bound to other carriers studied by our group, such as mitochondria penetrating peptides (mtDFO) or TAMRA-labeled mtDFO, where IC50 values ranged between 4 and 80 μmol L^{-1} (Alta et al. 2017).

Cell permeation studies

Because candidate chelators for the remobilization of bodily iron stores must also be able to cross biological membranes in order to access intracellular pools of labile iron while being orally active, TPP–DFO mitochondrial localization was studied. TPP–DFO is fluorescent (Fig. 4), which is useful for confocal microscopy tests. Considering only its autofluorescence, representative images revealing colocalization of the TPP–DFO with MitoTracker Deep Red in A2780 ovarian cancer cells are shown in Fig. 5.

This protocol is often used in mitochondrial localization assays for peptides linked to an orange fluorescent probe such as (2-[[1-(5-carboxypentyl)-4 (1H)-quinolinylidene] methyl]-3-methyl-benzothiazolium bromide)) (Kelley et al. 2011), which is

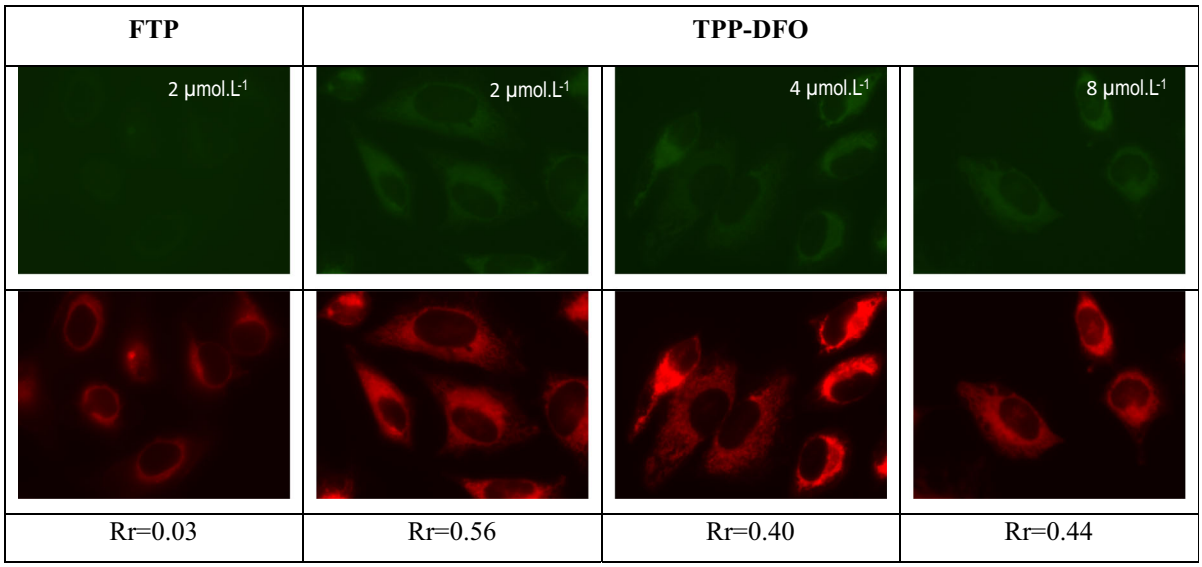

Fig. 5 Localization of TPP and TPP-DFO in A2780 Cells. Images collected for FTP and TPP-DFO were analyzed with an algorithm for the calculation of Rr (Pearson´s coefficient). Values reported were calculated from more than 100 cells analyzed in multiple (> 3) experiments

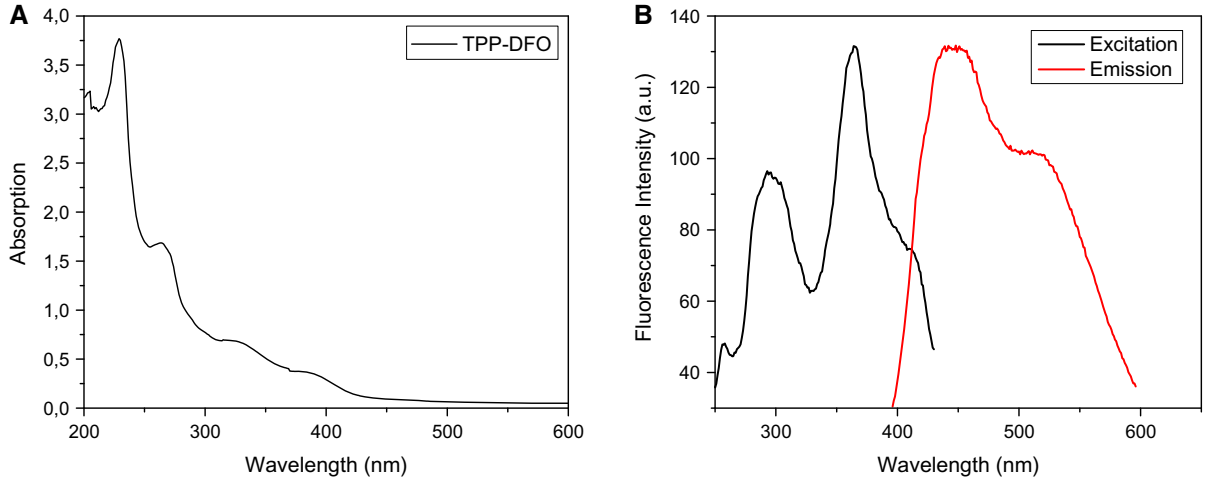

Fig. 6 Spectral features of TPP-DFO. (**a**) UV-absorption of 50 μmol L^{-1} TPP–DFO; (**b**) fluorescence spectra of 50 μmol L^{-1} TPP–DFO fluorescence excitation (λ_{Ex} = 365 nm) and emission (λ_{Em} = 445 nm)

excited at 488 nm and emits at 505–550 nm. For visualization of MitoTracker Deep Red 633 nm, emission was collected with a long pass filter at 560 nm. Even though this is not the optimal excitation/emission pair for TPP–DFO (Fig. 4), good Pearson's correlation coefficients (Rr) for the colocalization of both dyes in A2780 cells were obtained (Table 1A, Supplementary Information). TPP–DFO localizes in the mitochondria with Rr ranging from 0.40 to 0.56, which is comparable to other mitochondria-targeted versions of DFO (Rr 0.45–0.68) (Alta et al. 2017).

Incubation for 60 min gave the best colocalization images, but the same profiles were obtained at shorter (15 or 30 min) incubation periods (data not shown). Increase of TPP–DFO concentration led to a progressive decrease of Rr, related to the compromise of mitochondrial function as TPP positive charge can lead to membrane depolarization (Kelso et al. 2001). Also, some dyes or probes are capable of interfering with the electron transport chain to reduce respiration (Yousif et al. 2009). Therefore, delivery applications based on this type of transporter must include careful monitoring of cellular toxicity (Yousif et al. 2009). Cancer cells display an increased mitochondrial membrane potential compared to normal cells; this hyperpolarization increases the uptake of DLCs, providing a degree of selective targeting (Pathania et al. 2009). Mitochondrial uptake of TPP–DFO is dependent on membrane potential. The large $\Delta\Psi m$ is considered as the main reason for the selectivity and specificity of TPP-DFO.

Different mitochondrial vectors (peptides or TPP) for cargo transport to the same cell line A2780 can be used. TPP-bound cargoes are loaded to mitochondria with almost the same specificity than peptide-bound cargoes (Alta et al. 2017), indicating that the TPP-DFO impart a high degree of specificity (Horton and Kelley 2009; Mourtada et al. 2013; Wisnovsky et al. 2013). On the other hand, peptide-based conjugates synthesis is more expensive and complex than TPP-DFO synthesis. Also, TPP-DFO purification is simpler owing to a lower percentage of byproducts present in its crude form. Together with its good water solubility and low cytotoxicity, TPP-DFO is a very convenient tool for long-term labeling and tracking of iron in mitochondria (Fig. 6).

Conclusions

We described the synthesis and characterization of the first siderophore targeted to mitochondria with the TPP vector. TPP-DFO, based on a delocalized lipophilic cation scaffold, possesses characteristics conducive to its use as a delivery vector: simple and straightforward synthesis, facile derivatization, and biocompatibility. In this study, we showed that the conjugate preserved the iron chelation ability and antioxidant activity of parent DFO, besides being

relatively non-toxic and displaying good mitochondrial localization. Thus, TPP-DFO may be a useful chelator for iron redistribution therapy and an example of a class of effective mitochondrial transporters that are suited to traverse a difficult to penetrate organelle membrane.

Acknowledgements This work was supported by CAPES, FAPESP and CNPq (Brazilian government agencies). The authors thank Dr. Cleber Wanderlei Liria for discussions and technical assistance.

Compliance with ethical standards

Conflict of interest The authors declare no conflict of interests.

References

Abián J, Carrascal M, Gay M (2008) Introducción a la Espectrometría de masas para la caracterización de Péptidos y proteínas en Proteómica. Sepro 2:16–34

Alta ECP, Goswami D, Machini MT et al (2014) Desferrioxamine-caffeine (DFCAF) as a cell permeant moderator of the oxidative stress caused by iron overload. Biometals 27:1351–1360. doi:10.1007/s10534-014-9795-7

Alta RYP, Vitorino HA, Goswami D et al (2017) Mitochondria-penetrating peptides conjugated to desferrioxamine as chelators for mitochondrial labile iron. PLoS ONE 12: e0171729. doi:10.1371/journal.pone.0171729

Baccan MM, Chiarelli-Neto O, Pereira RMS, Espósito BP (2012) Quercetin as a shuttle for labile iron. J Inorg Biochem 107:34–39. doi:10.1016/j.jinorgbio.2011.11.014

Cabantchik ZI (2014) Labile iron in cells and body fluids: physiology, pathology, and pharmacology. Front Pharmacol 5:1–11. doi:10.3389/fphar.2014.00045

Domagal-Goldaman SD, Paul KW, Sparks DL, Kubicki JD (2009) Quantum chemical study of the Fe(III)-deferrioxamine B siderophore complex-Electronic structure, vibrational frecuencies, and equilibrium Fe-isotope fractionation. Geochim Cosmochim Acta 73:1–12

Esposito BP et al (2003) Labile plasma iron in iron overload: redox activity and susceptibility to chelation. Blood 102:2670–2677. doi:10.1182/blood-2003-03-0807

Espósito BP, Epsztejn S, Breuer W, Cabantchik ZI (2002) A review of fluorescence methods for assessing labile iron in cells and biological fluids. Anal Biochem 304:1–18. doi: 10.1006/abio.2002.5611

Filipovska A, Kelso GF, Brown SE et al (2005) Synthesis and characterization of a triphenylphosphonium-conjugated peroxidase mimetic: insights into the interaction of ebselen with mitochondria. J Biol Chem 280:24113–24126. doi:10.1074/jbc.M501148200

Fonseca SB, Pereira MP, Mourtada R et al (2011) Rerouting chlorambucil to mitochondria combats drug deactivation and resistance in cancer cells. Chem Biol 18:445–453. doi:10.1016/j.chembiol.2011.02.010

Goswami D, Machini MT, Silvestre DM et al (2014) Cell penetrating peptide (CPP)-conjugated desferrioxamine for enhanced neuroprotection: synthesis and in vitro evaluation. Bioconjugate Chem 25:2067–2080. doi:10.1021/bc5004197

Goswami D, Vitorino HA, Alta RYP et al (2015) Deferasirox-TAT(47–57) peptide conjugate as a water soluble, bifunctional iron chelator with potential use in neuromedicine. Biometals 28:869–877. doi:10.1007/s10534-015-9873-5

Gottlieb HE, Kotlyar V, Nudelman A (1997) NMR chemical shifts of common laboratory solvents as trace impurities. J Org Chem 62:7512–7515

Horton KL, Kelley SO (2009) Engineered apoptosis-inducing peptides with enhanced mitochondrial localization and potency. J Med Chem 52:3293–3299. doi:10.1021/jm900178n

Horton KL, Stewart KM, Fonseca SB et al (2008) Mitochondria-penetrating peptides. Chem Biol 15:375–382. doi: 10.1016/j.chembiol.2008.03.015

Kalinowski D, Richardson D (2005) The evolution of iron chelators for the treatment of iron overload disease and cancer. Pharmacol Rev 57:547–583. doi:10.1124/pr.57.4.2.547

Kelley SO, Stewart KM, Mourtada R (2011) Development of novel peptides for mitochondrial drug delivery: amino acids featuring delocalized lipophilic cations. Pharm Res 28:2808–2819. doi:10.1007/s11095-011-0530-6

Kelso GF, Porteous CM, Coulter CV et al (2001) Selective targeting of a redox-active ubiquinone to mitochondria within cells: antioxidant and antiapoptotic properties. J Biol Chem 276:4588–4596. doi:10.1074/jbc.M009093200

Kolevzon N, Kuflik U, Shmuel M et al (2011) Multiple triphenylphosphonium cations as a platform for the delivery of a pro-apoptotic peptide. Pharm Res 28:2780–2789. doi:10.1007/s11095-011-0494-6

Lei W, Xie J, Hou Y et al (2010) Mitochondria-targeting properties and photodynamic activities of porphyrin derivatives bearing cationic pendant. J Photochem Photobiol B 98:167–171. doi:10.1016/j.jphotobiol.2009.12.003

Liberman EA, Topaly VP, Tsofina LM et al (1969) Mechanism of coupling of oxidative phosphorylation and the membrane potential of mitochondria. Nature 222:1076–1078

Liu J, Obando D, Schipanski LG et al (2010) Conjugates of desferrioxamine B (DFOB) with derivatives of adamantane or with orally available chelators as potential agents for treating iron overload. J Med Chem 53:1370–1382. doi:10.1021/jm9016703

Lou P-H, Hansen BS, Olsen PH et al (2007) Mitochondrial uncouplers with an extraordinary dynamic range. Biochem J 407:129–140. doi:10.1042/BJ20070606

Ma Y, Abbate V, Hider RC (2014) Iron-sensitive fluorescent probes: monitoring intracellular iron pools. Metallomics 7:212–222. doi:10.1039/c4mt00214h

Malouitre S, Dube H, Selwood D, Crompton M (2010) Mitochondrial targeting of cyclosporin A enables selective inhibition of cyclophilin-D and enhanced cytoprotection after glucose and oxygen deprivation. Biochem J 425:137–148. doi:10.1042/BJ20090332

Mourtada R, Fonseca SB, Wisnovsky SP et al (2013) Re-directing an alkylating agent to mitochondria alters drug target and cell death mechanism. PLoS ONE 8:1–9. doi:10.1371/journal.pone.0060253

Murphy MP, Smith RA (2000) Drug delivery to mitochondria: the key to mitochondrial medicine. Adv Drug Deliv Rev 41:235–250

Murphy MP, Smith RAJ (2007) Targeting antioxidants to mitochondria by conjugation to lipophilic cations. Annu Rev Pharmacol Toxicol 47:629–656. doi:10.1146/annurev.pharmtox.47.120505.105110

Nishikawa T, Edelstein D, Du XL et al (2000) Normalizing mitochondrial superoxide production blocks three pathways of hyperglycaemic damage. Nature 404:787–790. doi:10.1038/35008121

Pathania D, Millard M, Neamati N (2009) Opportunities in discovery and delivery of anticancer drugs targeting mitochondria and cancer cell metabolism. Adv Drug Deliv Rev 61:1250–1275. doi:10.1016/j.addr.2009.05.010

Pitkanen S, Robinson BH (1996) Mitochondrial complex I deficiency leads to increased production of superoxide radicals and induction of superoxide dismutase. J Clin Investig 98:345–351. doi:10.1172/JCI118798

Puccio H, Simon D, Cossée M et al (2001) Mouse models for Friedreich ataxia exhibit cardiomyopathy, sensory nerve defect and Fe-S enzyme deficiency followed by intramitochondrial iron deposits. Nat Genet 27:181–186. doi:10.1038/84818

Rin Jean S, Tulumello DV, Wisnovsky SP et al (2014) Molecular vehicles for mitochondrial chemical biology and drug delivery. ACS Chem Biol 9:323–333. doi:10.1021/cb400821p

Ross MF, Filipovska A, Smith RAJ et al (2004) Cell-penetrating peptides do not cross mitochondrial membranes even when conjugated to a lipophilic cation: evidence against direct passage through phospholipid bilayers. Biochem J 383:457–468. doi:10.1042/BJ20041095

Ross MF, Kelso GF, Blaikie FH et al (2005) Lipophilic triphenylphosphonium cations as tools in mitochondrial bioenergetics and free radical biology. Biochemistry 70:222–230. doi:10.1007/s10541-005-0104-5

Smith RAJ, Kelso GF, Blaikie FH et al (2003a) Using mitochondria-targeted molecules to study mitochondrial radical production and its consequences. Biochem Soc Trans 31:1295–1299. doi:10.1042/BST0311295

Smith RAJ, Porteous CM, Gane AM, Murphy MP (2003b) Delivery of bioactive molecules to mitochondria in vivo. Proc Natl Acad Sci USA 100:5407–5412. doi:10.1073/pnas.0931245100

Smith RAJ, Hartley RC, Murphy MP (2011) Mitochondria-targeted small molecule therapeutics and probes. Antioxid Redox Signal 15:3021–3038. doi:10.1089/ars.2011.3969

Smith RAJ, Hartley RC, Cochemé HM, Murphy MP (2012) Mitochondrial pharmacology. Trends Pharmacol Sci 33:341–352. doi:10.1016/j.tips.2012.03.010

Suresh R, Kamalakkannan D, Ranganathan K et al (2013) Solvent-free synthesis, spectral correlations and antimicrobial activities of some aryl imines. Spectrochim Acta 101:239–248. doi:10.1016/j.saa.2012.09.039

Vitorino HA, Mantovanelli L, Zanotto FP, Espósito BP (2015) Iron metallodrugs: stability, redox activity and toxicity against Artemia salina. PLoS ONE 10:e0121997. doi:10.1371/journal.pone.0121997

Wade LG (2003) Aminoacids, peptides and proteins. Organic chemistry, 5th edn. Pearson Prentice Hall, Pearson, pp 1145–1151

Waters (1999) Background Ion List for ESI. Tech Note 1–4

Wilson JJ, Lippard SJ (2012) In vitro anticancer activity of cis -diammineplatinum(II) complexes with β-diketonate leaving group ligands. J Med Chem 55:5326–5336. doi:10.1021/jm3002857

Wisnovsky SP, Wilson JJ, Radford RJ et al (2013) Targeting mitochondrial DNA with a platinum-based anticancer agent. Chem Biol 20:1323–1328. doi:10.1016/j.chembiol.2013.08.010

Wittig G, Schoch-Grübler U (1978) Kombination von Carbonyl-Olefinierungsreaktion und gezielter Aldolkondensation. Eur J Org Chem 2:362–375

Yousif LF, Stewart KM, Kelley SO (2009) Targeting mitochondria with organelle-specific compounds: strategies and applications. ChemBioChem 10:1939–1950. doi:10.1002/cbic.200900185